RESEARCH ARTICLE

Optimization of polyurethane-bonded thin overlay mixture designation for airport pavement

Xianrui LI[a], Ling XU[a*], Qidi ZONG[a], Fu JIANG[b], Xinyao YU[b], Jun WANG[c], Feipeng XIAO[a*]

[a] Key Laboratory of Road and Traffic Engineering of Ministry of Education, Tongji University, Shanghai 201804, China

[b] CAAC East China Regional Administration, Shanghai 200335, China

[c] Ningbo Airport Group Co., Ltd., Ningbo 315154, China

*Corresponding authors. E-mails: lxu@tongji.edu.cn; fpxiao@tongji.edu.cn

ABSTRACT This research explored the application potential of PUM thin-overlay technology on airport rapid maintenance. The rapid curing process of polyurethane binder determines the limited time window for mixing and construction of polyurethane-bonded mixture (PUM), which presents significant difference with hot-mix asphalt (HMA) technology. Therefore, this research investigated and optimized the mix design of PUM for airport thin-overlay technology based on its thermosetting characteristics. First, limestone and basalt were comprehensively compared as an aggregate for PUM. Then, the effects of molding and curing conditions were studied in terms of mixing time, molding method, molding parameters and curing temperature. Statistical analysis was also conducted to evaluate the effects of gradation and particle size on PUM performances based on gray relational analysis (GRA), thus determining the key particle size to control PUM performances. Finally, the internal structural details of PUM were captured by X-ray CT scan test. The results demonstrated that it only took 12 hours to reach 75% of maximum strength at a curing temperature of 50 °C, indicating an efficient curing process and in turn allowing short traffic delay. The internal structural details of PUM presented distribution of tiny pores with few connective voids, guaranteeing waterproof property and high strength.

KEYWORDS polyurethane-bonded mixture, mix design optimization, airport pavement, thin overlay, gray relational analysis

1 Introduction

In the pavement engineering field, the service-ability of pavements, especially airport runways, is highly dependent on the raw material quality for construction and maintenance [1]. Due to the stability and compressive resistance, cement concrete pavement is widely applied to airport pavement. However, after being exposed to repeated aircraft loads and long-term effects of environmental factors, the airport pavement surface deteriorates gradually during service life [2]. Because cement concrete is brittle and the soil foundation is relatively sensitive to uneven settlement and overloading, the pavement deterioration can, later, develop rapidly. Various airport pavement problems have included cracking, pockmarked surfaces, pits, corner breaking, and

peeling caused by salt freezing [3], as showed in Fig. 1. Airport pavement maintenance should meet the challenges of higher cost, longer maintenance period and flight traffic delay. Generally, asphalt materials have been adopted to repair early cracking and delay damage [4]. Asphalt mixture can be applied to form a composite pavement surface when pavement is severely damaged. At present, this kind of "white + black" overlay technology is commonly adopted on airport pavements [5].

However, from the chemical and physical perspective, asphalt materials suffer performance deterioration and chemical components change inevitably under the combined effects of light, heat and water [6]. As a result, the asphalt materials service life is relatively short and various forms of distress (e.g., rutting, shifting and reflection cracking) are prone to occur before its designed life end [7]. Repeated asphalt pavement overlay
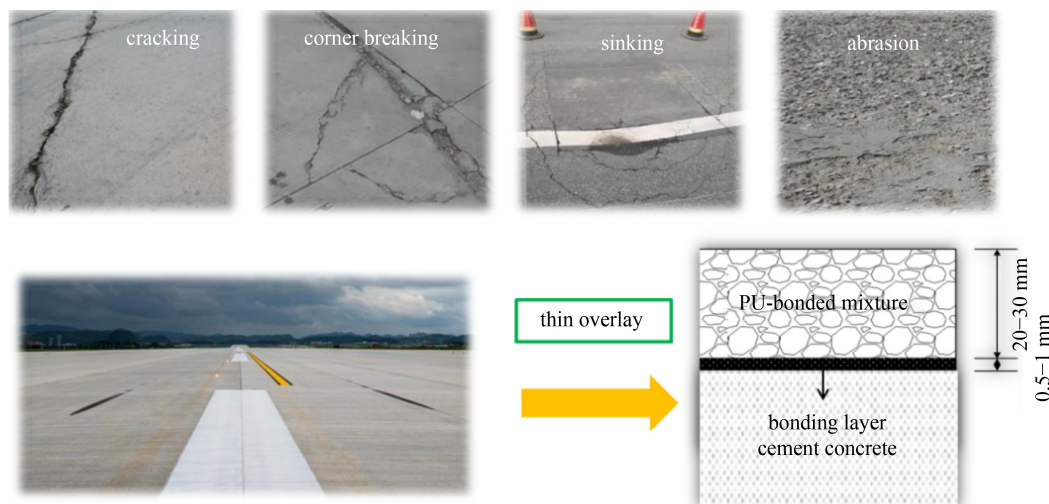
Fig. 1   Concrete pavement diseases of airport runway and thin overlay maintenance technology.

maintenance also affects the overall operation of busy airports, reducing their social and economic benefits [8]. The commonly applied maintenance materials, namely asphalt and Portland cement, are still unable to satisfy the high requirements for airport pavement. Therefore, it is urgent to propose new materials and new processes to solve the current challenges of airport pavement maintenance.

Polymer materials are defined as extremely long molecules with countless repeat units in basic chains. Polymer technology is a growth area in civil infrastructure and construction, a huge variety of polymers has been applied widely in construction and building engineering. Such polymers include Styrene-Butadiene-Styrene (SBS), Epoxy Resins (ER), rubber, Polyvinyl chloride (PVC), Polyethylene (PE), Ethyl Vinyl Acetate (EVA), Styrene-Butadiene-Rubber (SBR) and so on [9,10]. Among them, polyurethane (PU) is defined as a material with carbamate groups in polymer molecules, and is generally synthesized from the chemical reactions between polyether polyols and isocyanates [11]. As a kind of organic polymer material, polyurethane presents excellent properties for various application markets. Such properties include elongation, thermal stability, chemical resistance, energy absorption and corrosion resistance [12].

At present, various polyurethane products on market are mainly classified into elastomers, foams, adhesives, coatings, sealants and waterproof materials, meeting various application demands [13,14]. Thanks to the excellent properties, polyurethane (PU) has attracted extensive interests of pavement researchers and authorities worldwide [15,16].

Polyurethane in pavement engineering as a partial or complete replacement of conventional materials has gaining popularity in engineering recently [17,18]. Therefore, researchers have attempted to employ polyurethane adhesive, polyurethane-bonded mixture (PUM), as binder to replace asphalt materials completely [19]. PUM uses polymer adhesive to bond aggregates together and the cured polyurethane material forms a three-dimensional cross-linked network structure, which has high bonding strength and thermal stability [20]. Compared with traditional cement concrete, polyurethane material, owning the superior bonding properties, has advantages in terms of strength, rutting resistance, durability and moisture resistance [12]. In addition, polyurethane material with shorter curing time can be used for reducing traffic closure time and flight traffic delays. Therefore, thin-overlay technology with PUM presents great potential for rapid maintenance of airport pavements.

Due to the favorable properties of polyurethane binder, PUM can be expected to extend service life and improve performance of pavements. Indeed, PUM was designed to achieve special aspects of functional pavements, in terms of permeability [21,22], anti-skid, de-icing [23], noise reduction [24] and so on. Correspondingly, PUM has been mainly applied as porous polyurethane mixture (PPM) [25], open-graded friction course (OGFC) [26], self-stressing de-icing mixture and poroelastic road surface (PERS) [24,27]. Specifically, OGFC with PU presents higher strength, better skid resistance, rutting and fatigue resistance than ordinary asphalt mixture [26]. PPM generally adopts single size aggregate without fine aggregate. So, the air void of PPM is usually larger than 30%, and is mainly applied for permeable pavement [28]. Due to the larger porosity, PPM shows stronger abilities of noise reduction and anti-blocking, but its durability needs further investigation [25]. Chen et al. [23] prepared AC-13 PUM with good elastic deformability to achieve de-icing effect. They reported that PUM presented similar thermal conductivity and higher specific heat compared with asphalt mixture, which could provide better de-icing and anti-freezing property of pavement in cold areas.

In conclusion, PUM with excellent performances has been widely applied on functional pavements. However, the application of PUM as maintenance material for airport pavement thin-overlay technology is still in the exploratory stage. Besides, the mix designs of such porous PUM with high void ratio are proposed for landscape roads and non-motor vehicle lanes [12,19], which are not suitable for thin-overlay maintenance of airport pavement. Considering the thermosetting characteristics of PU binder, the molding and curing process also plays a vital role in the mix design of PUM, which presents significant difference from hot-mix asphalt (HMA) mixture.

Therefore, the main objective of this research was to investigate and optimize the mix design of PUM for airport thin-overlay technology. First, limestone and basalt were comprehensively compared as aggregate for PUM. Then, the effects of molding and curing condition were studied in terms of mixing time, molding parameter, molding method and curing temperature. Statistical analysis was conducted to evaluate the effects of gradation and particle size on PUM performances based on gray relational analysis (GRA). Finally, internal structural details of PUM were captured through X-ray CT scan.

2   Materials and methods

2.1   Materials

2.1.1   Isocyanate and polyether polyols

Polyurethane was formed by diols/polyols (A component) and di/poly isocyanates (B component) through chemical reaction, in the presence of catalysts, crosslinking agents, chain extenders. The molecular structures of two components are presented in Fig. 2, showing repeated urethane groups. The optimum component ratio of polyether polyols and isocyanate was 3:4 and the basic properties of polyurethane binder after curing process are shown in Table 1.

2.1.2   Aggregates

To compare the performances of limestone and basalt for PUM, the coarse aggregates 3.0−5.0 mm and 5.0−10.0 mm both included basalt and limestone, while fine aggregate 0−3.0 mm was limestone. The technical performance indicators of coarse and fine aggregates are shown in Table 2, referring to the specification JTG E42-2005.

2.2   Test methods

2.2.1   Volumetric characteristics test

In general, the volumetric characteristics of mixture affect the pavement durability significantly. Vacuum sealing method was adopted to measure the bulk density of PUM according to JTG E20-2011. The air void and theoretical maximum density of PUM were calculated according to JTG F40-2004.

2.2.2   Marshall stability test

According to JTG E20-2011, the Marshall stability test was adopted to evaluate the stability of PUM at high temperature. A Marshall sample was placed in a constant temperature water bath at 60 °C for 30 min and the linear loading speed of stability test was set at 50 mm/min.

2.2.3   Freeze-thaw split test

The freeze-thaw splitting test was carried out according to
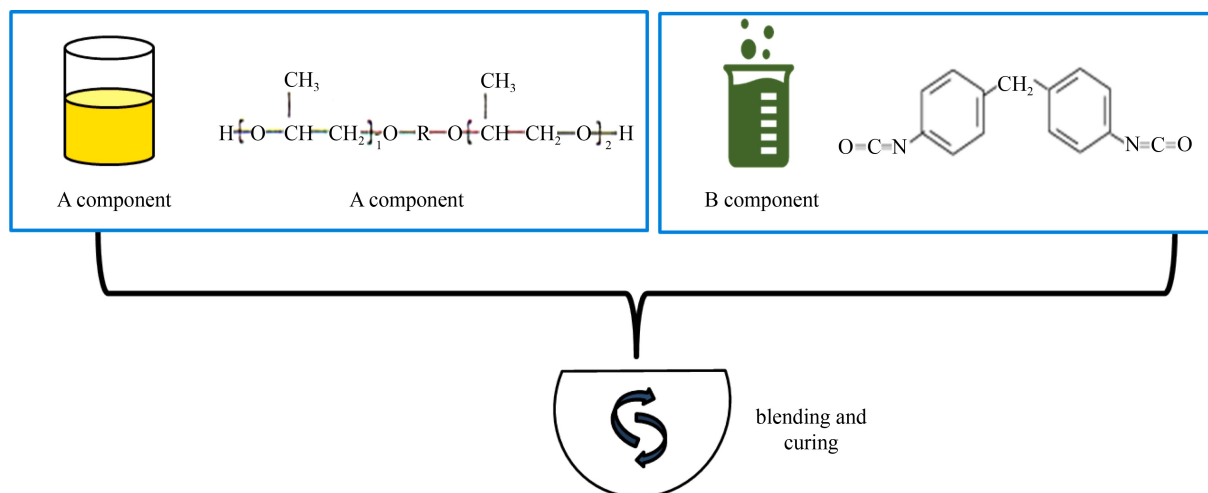

Fig. 2   Molecular formulas of isocyanate and polyether polyols.

the specification JTG E20-2011 T0729. Three specimens went through water saturation and freezing processes, while the other group of specimens was not processed. According to the splitting strength before and after freezing and thawing, the freeze-thaw splitting strength ratio (Tensile Strength Ratio, *TSR*) was calculated to evaluate the moisture resistance of the PUM.

$$TSR = \frac{R_{T1}}{R_{T2}} \times 100, \qquad (1)$$

where R_{T1} was the average value of splitting strength before freezing and thawing, MPa; R_{T2} was the average value of splitting strength after freezing and thawing, MPa; *TSR* was the freeze-thaw splitting strength ratio, %.

2.2.4 Cantanbro stripping test

According to specification JTG E20-2011 T0733, a Cantanbro stripping test was adopted to evaluate the bonding property between binder and aggregate in PUM. The quality loss of mixture specimen was measured to characterize the degree of aggregate shedding and loss after rotating and impacting, expressed as a percentage.

2.2.5 Mechanical strength test

According to JTG E30-2005, compressive strength test was carried out to measure the deformation resistance of PUM to wheel loads. Axial compressive strength with unconfined constraints (in MPa) was recorded. Flexural-tensile strength test was also conducted to measure the tensile strength (*TS*) elongation at break (E_b) of the mixture.

2.2.6 X-ray CT scan test

X-ray CT scan test was performed to capture the internal structural details of PUM. Y.CT Precision 2 (produced by YXLON Company) with 210.00 kV X-ray voltage and 0.32 mA current was adopted. The numbers of Image Dimension and Detector Pixel were both set at 2048 pixels. Professional software VG MAX 3.3 was used for image processing.

3 Results and discussion

3.1 Initial polyurethane binder calculation

The initial mix design of PUM adopted PUM-10 gradation, which was similar to AC-10 (a common gradation of mixture). The lower grading limit, upper grading limit and initial gradation of PUM-10 for PUM are shown in Fig. 3. The initial binder content was estimated based on the effective polyurethane film thickness, referring to the JTG F40-2004. The calculation results of polyurethane film thickness were calculated based on Eqs. (2) and (3), presented in Table 3 below.

$$SA = \sum (P_i \times FA_i), \qquad (2)$$

$$DA = \frac{P_{be}}{\gamma_b \times SA} \times 10, \qquad (3)$$

where *SA* was the specific surface area of aggregate, m²/kg; P_i was the passing rate of each sieve aggregate, %; FA_i was the surface area coefficient of aggregates with various particle sizes; *DA* was the effective thickness of

Table 1 Basic properties of polyurethane

properties	unit	value
tensile strength	MPa	43.0
elongation at break	%	28.5
elastic modulus	N/mm²	1966
tearing strength	MPa	127.2
shore hardness	D	68

Table 2 Basic properties of coarse and fine aggregates

parameters	basalt 5−10 mm	basalt 3−5 mm	limestone 5−10 mm	limestone 3−5 mm	limestone 0−3 mm	requirement	method
apparent specific density	3.048	2.999	2.748	2.755	2.674	–	
surface dry specific density	2.963	2.924	2.704	2.715	2.602	–	T 0308
bulk density	2.922	2.887	2.679	2.693	2.561	–	
water absorption (%)	1.41	1.30	0.93	0.84	1.59	–	
crushing value (%)	10.1	–	12.7	–	–	≤20	T 0316
LA abrasion loss (%)	10.6	10.5	12.5	12.6	–	≤28	T 0323
needle-like content (%)	7.4	–	11.2	–	–	≤15	T 0312
particle content (< 0.075 mm)	1..0	0.6	1.3	1.7	–	≤1	T 0310
soft stone content	1.3	–	1.2	–	–	≤2	T 0320
hardness	1.44	0.79	1.76	1.28	1.50	≤10	T 0320 T 0340

polyurethane adhesive film, μm; P_{be} was the amount of polyurethane binder, %; $γ_b$ was the relative density of polyurethane cement at 25 °C, which was measured as 1.02;

Referring to the study of binder thickness of the asphalt mixture, the minimum thickness of the polyurethane binder film was set to 20 μm. The amount of binder (P_{be}) was calculated as 8.6% of the mixture according to the formula ($DA = 20$ μm) and therefore the initial polyurethane binder dosage was determined as 9%.

3.2   Mixture optimization of aggregate type

Limestone and basalt, provided by local contractor, were compared to evaluate the effect of aggregate type on PUM performances, covering bulk density, air void, Marshall stability, splitting strength, tensile strength ratio, theoretical maximum density, stripping degree, ultimate TS and E_b. These parameters were gathered together with a radar map, as presented in Fig. 3. All data were normalized and divided by the parameters of basalt aggregate to achieve coordinate axis normalization.

It was found that PUM with basalt presented higher normalized values than limestone, indicating better deformation resistance, bonding ability and moisture
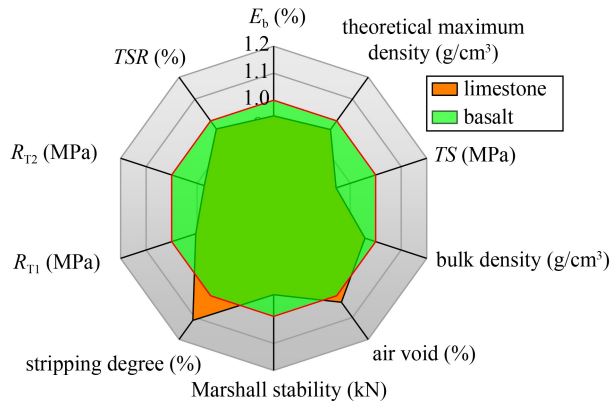

Fig. 3   Performances comparison between limestone and basalt for PUM.

stability. In addition, image processing was performed on the cross section of one common specimen to quantitatively identify the interface fracture mode of PUM. As illustrated in Fig. 4, the proportion of aggregate fracture with more exposed aggregate surfaces for limestone was higher than for basalt, resulting from poor cohesion between polyurethane binder and limestone. In summary, basalt was more suitable as the aggregate because of the better bonding strength with polyurethane binder.

3.3   Mixture optimization of molding and curing condition

3.3.1   Effect of mixing duration

Here, 0, 30, 60, and 90 s dry-mixed durations for aggregate and 30, 60, 90, 120 s wet-mixed durations were selected to determine the optimal mixing process parameters. PUM was produced through mixing the aggregates, polyols and isocyanates at room temperature (25 °C). The properties of PUM with different mixing durations are shown in Fig. 5.

After the 90 s wet-mixed duration, then the longer dry-mixed duration with more uniform aggregates enhanced bonding strength and denser structure of PUM. Similarly, after the 60 s dry-mixed duration, then the longer wet-mixed duration resulted in more uniform wrapping between aggregate and polyurethane binder, decreased air voids and higher strength. Considering the mechanical energy consumption and mixture performance improvement efficiency, 60 s dry-mixed duration for aggregate and 60 s wet-mixed duration for mixture were combined as the recommended mixing duration parameters.

3.3.2   Effect of molding parameter

Effects of molding parameters for different molding methods were investigated, including Marshall hitting, Surperpave Gyration Compaction (SGC), artificial molding and vibratory compaction method.

For the Marshall hitting method, measurements were

Table 3   Calculation results of polyurethane film thickness

sieve size (mm)	lower limit	passing percentage (%)	upper limit	surface area coefficient	specific surface area (m²/kg)
13.2	100	100.0	100	0.0041	0.4100
9.5	95	98.6	100	0.0041	0.4041
4.75	60	71.6	88	0.0041	0.2934
2.36	35	50.0	72	0.0082	0.4100
1.18	20	35.0	61	0.0164	0.5740
0.6	12	25.0	50	0.0287	0.7175
0.3	6	15.0	22	0.0614	0.9210
0.15	3	3.9	10	0.1229	0.4845

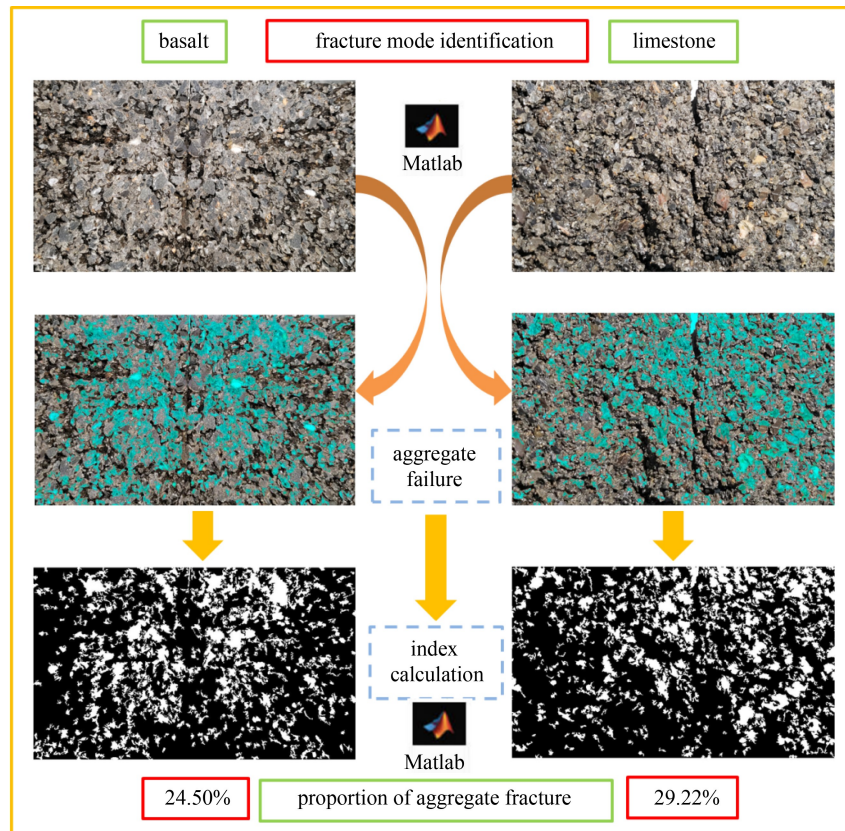Note: The total specific surface area S_A was 4.2144 m²/kg.

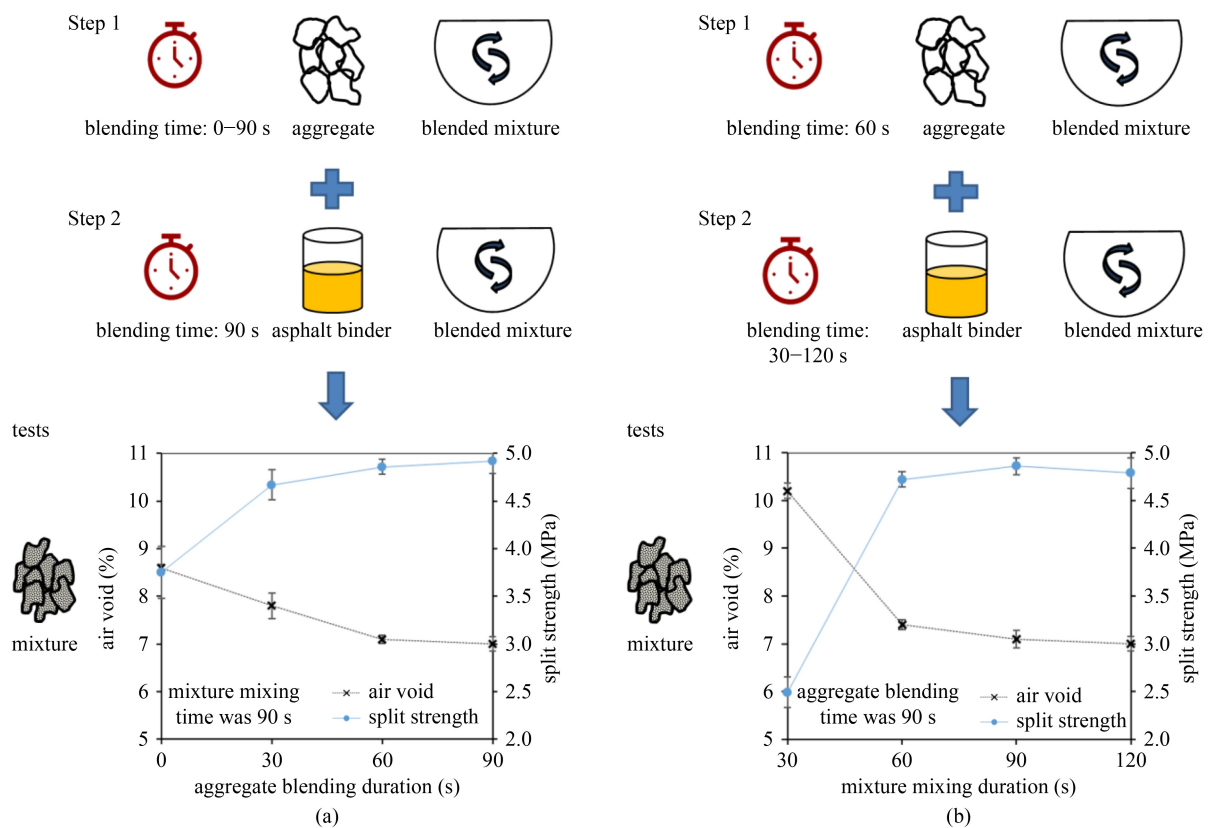**Fig. 4**   Fracture mode identification of limestone and basalt for PUM.

Fig. 5   Properties of PUM with different mixing duration. (a) Aggregate blending duration; (b) mixture mixing duration.

made of volumetric characteristics, Marshall stability and splitting tensile strength according to different interpose times and compaction times, as presented in Fig. 6. Results showed that the increase of interpose times and compaction times would promote the denser structure formation with higher bulk density and lower air voids. Meanwhile, mechanical property was also improved with higher Marshall stability and splitting tensile strength. Considering the limited improvement in efficiency of mixture performance, 15 interpose times and 50 compaction times were determined as the optimized molding parameters for the Marshall hitting method.

For the gyration compaction method, the SGC parameters were investigated with the compaction strength of 600 kPa, rotation speed of 30 revolutions/min and compaction angle of 1.25°. The sample height and calculated bulk density of PUM were recorded as shown in Fig. 7. In order to compare the performances of PUM under different rotation compaction times, air void and splitting strength were measured under 10, 20, and 30 rotation compaction times respectively.

For 10 rotation compaction times, the void ratio of PUM reached 9.5% and the splitting strength was lower than 3 MPa, indicating poor performance. Longer rotation compaction time with pressure produced tighter adhesion between aggregate and polyurethane binder. Therefore, 30 rotation compaction times were recommended as the molding parameters of the SGC with 4.3% air void.

For the artificial molding method with various interpose times, Marshall cylindrical specimens were used to measure air void and splitting strength while cubic specimens were used to determine the compressive strength. As shown in Fig. 8(a), the air void ratio of specimen gradually decreased while the compressive and splitting strength gradually enhanced with the increase of interpose time. The specimen reached a dense and compact state under the action of 45 interposes, which was therefore recommended as the molding parameter.

For the vibratory compaction method, a concrete vibrating compactor with 370 W power and 2840 r·min^{-1} vibration frequency was used to mold mixture specimens. Performance comparison of PUM with different vibration duration is presented in Fig. 8(b). After the vibration duration reached 1 min, the air void, splitting strength and compressive strength no longer changed significantly, indicating a dense structure of specimens.
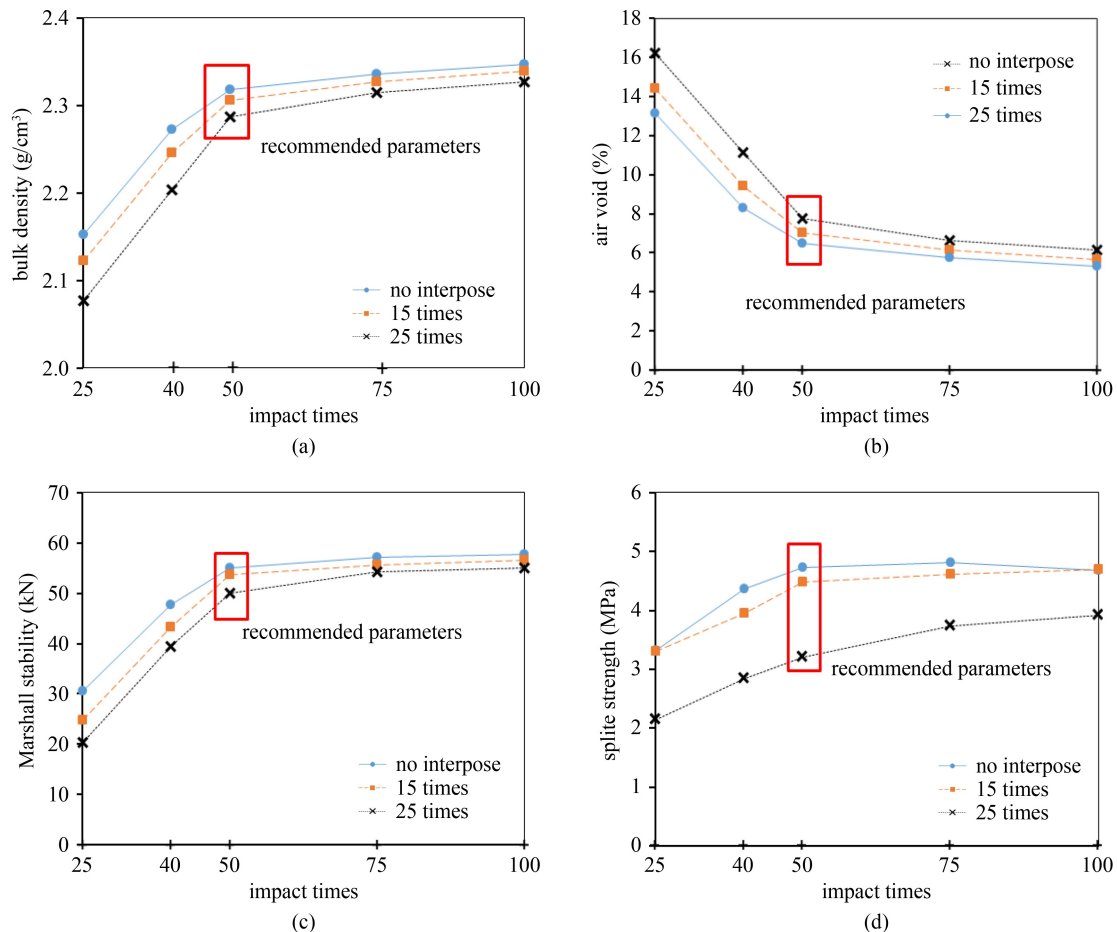

Fig. 6 Properties of PUM with different interpose times and compaction times. (a) Bulk density; (b) air void; (c) Marshall stability; (d) splitting tensile strength.
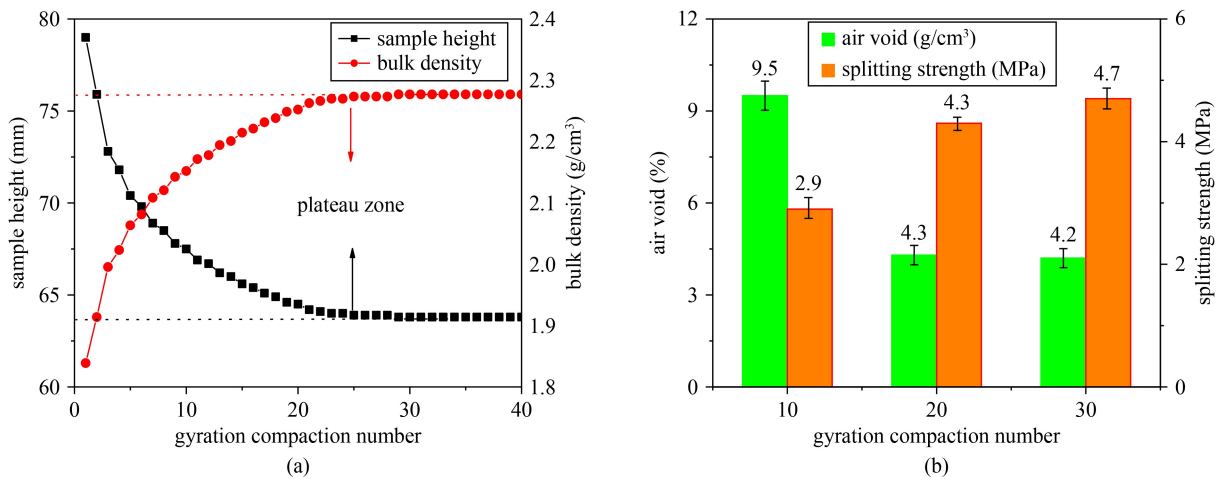
Fig. 7 Comparison of PUM under different rotation compaction times. (a) Sample height and bulk density; (b) air void and split strength.
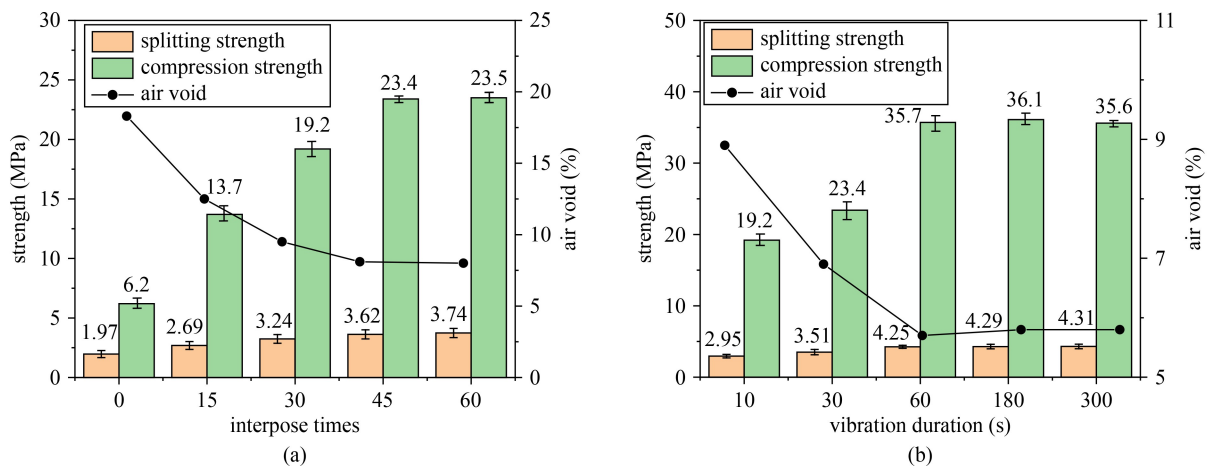

Fig. 8 Performance comparison of PUM. (a) Interpose times; (b) vibration duration.

According to the test results above, the optimum parameters for four molding methods were determined as summarized below.

1) Marshall hitting method: 15 interpose times and 50 compaction times;

2) surperpave gyration compaction: 30 rotation compaction times;

3) artificial molding method: 45 interposes;

4) vibratory compaction method: 1 minute vibration duration.

3.3.3   Molding method optimization

In order to compare the difference of four molding methods with corresponding optimal molding parameters, comprehensive performance evaluation was conducted in terms of air void, stripping degree, Marshall stability, flow value, splitting strength and freeze-thaw *TSR*. The most suitable molding method for PUM was determined by min–max range standardization, according to Eq. (4).

$$E_b = \frac{R_i - R_{min}}{R_{max} - R_{min}}, \qquad (4)$$

where E_b was the normalized value of test result, R_{max} was the optimum value, R_{min} was the worst value, R_i was the any value of indicator.

The test results and min–max range dimensionless results for PUM are presented in Fig. 9 and Table 4, respectively.

A larger standardized value denotes better comprehensive performance of PUM. As concluded from Table 4, the ranking evaluation was vibratory compaction method > Marshall hitting method > surperpave gyration compaction > artificial molding method. Therefore, the vibratory compaction method was recommended for molding PUM.

3.3.4   Effect of curing temperature

Considering the thermosetting characteristics of polyurethane, temperature would affect the curing characteristics
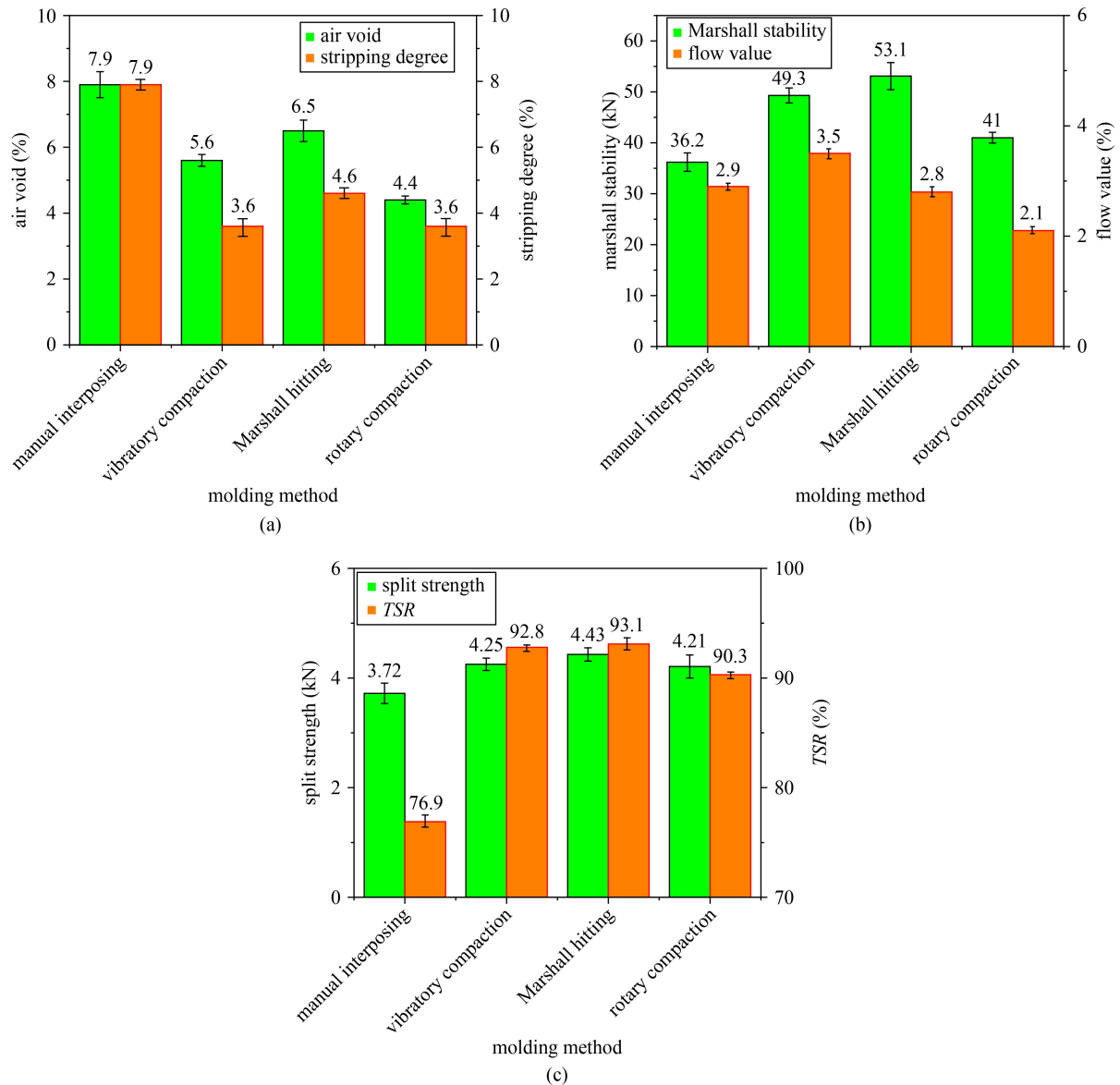
Fig. 9   Mixture performance evaluation of four molding methods. (a) Air void and stripping degree; (b) Marshall stability and flow value; (c) split strength and *TSR*.

Table 4   Min–max range dimensionless results of evaluation indicators

index	surperpave gyration compaction	Marshall hitting method	vibratory compaction method	artificial molding method
air void	1.00	0.40	0.66	0.00
Marshall stability	0.28	1.00	0.83	0.00
stripping degree	1.00	0.77	1.00	0.00
splitting strength	0.69	1.00	0.75	0.00
TSR	0.83	1.00	0.98	0.00
standardized sum	3.80	4.17	4.22	0.00

of polyurethane binder significantly. Therefore, the strength development of PUM was investigated at various temperatures. The curing temperatures of PUM from 10 to 50 °C were selected for application on Shanghai city covering the most common temperature conditions

occurring during the curing process. Meanwhile, the compression strength was measured at different curing duration as shown in Fig. 10.

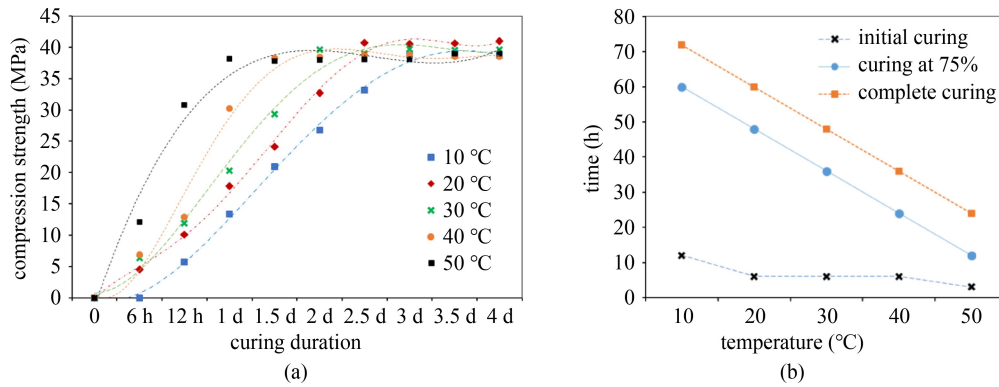During the curing time, the compressive strength of PUM was gradually increasing. Meanwhile, the rate of

Fig. 10 Compression strength development of mixture. (a) Curing durations; (b) curing temperatures.

compressive strength growth tended to decrease because the curing reaction of polyurethane binder was gradually completing. Curing temperature also had a significant effect on the strength formation.

In order to compare the curing rate more precisely, the durations to reach initial strength (3−10 MPa), 75% of the maximum strength and complete curing of PUM at different temperatures were recorded. It was observed that time and temperature presented a strong linear correlation for the durations to reach 75% of the maximum strength and complete curing. The curing rate was promoted by high temperature. It only took 12 h to reach 75% of the maximum strength at 50 °C, indicating efficient curing and light traffic delay.

3.4 Mixture optimization of gradation

3.4.1 Grey Relational Analysis

Grey Relational Analysis (GRA) was a statistical method to quantitatively analyze and compare the trend of a system. The steps for calculating the relevance degree were as follows.

1) Dimensionless processing of original data

Assuming that the original data had one evaluation object with m influencing factors, and each factor and object had n data sequences, the original data column was an $n \times (m + 1)$ matrix, which could be expressed as:

$$X = (x_{ij'})_{n \times (m+1)} = \begin{bmatrix} x_{10} & x_{11} & \cdots & x_{1m} \\ x_{20} & x_{21} & \cdots & x_{2m} \\ \vdots & \vdots & \cdots & \vdots \\ x_{n0} & x_{n1} & \cdots & x_{nm} \end{bmatrix}$$

$$(i = 1, 2, \cdots, n; \ j' = 0, 1, \cdots, m), \qquad (5)$$

For each set of data columns, the value was dimensionless in proportion to the 0−1 range. The calculation formula was as follows

$$u_{ij'} = \frac{x_{ij'} - \min(x_{j'})}{\max(x_{j'}) - \min(x_{j'})}. \qquad (6)$$

2) Determination of the comparison series and the reference series

Suppose the comparison series (the influence index) was $x_i = \{x_{ij} | i = 1, 2, \cdots, n; j = 1, 2, \cdots, m\}$ and the reference series (the evaluation object) was $x_0 = \{x_{i0} | i = 1, 2, \cdots, n\}$.

3) Determination of the corresponding weight of each impact indicator

The same weight $1/m$ was adopted for each of the influence indicators; that is, the final weighted grey correlation value was the average value of each grey correlation value.

4) Calculate the grey correlation coefficient ξ_{ij}

$$\xi_{ij} = \frac{\min\limits_{i} \min\limits_{j} |x_{0j} - x_{ij}| + \rho \max\limits_{i} \max\limits_{j} |x_{0j} - x_{ij}|}{|x_{0j} - x_{ij}| + \rho \max\limits_{i} \max\limits_{j} |x_{0j} - x_{ij}|}, \qquad (7)$$

where ξ_{ij} was the correlation coefficient of the comparison sequence x_i to the reference sequence x_0 on the j-th index, $|x_{0j} - x_{ij}|$ was the absolute difference between x_i and x_0 corresponding to the j-th index, $\min\limits_{i} \min\limits_{j} |x_{0j} - x_{ij}|$ was the minimum absolute difference between the two levels, and $\max\limits_{i} \max\limits_{j} |x_{0j} - x_{ij}|$ was the maximum absolute difference between two levels; $\rho \in (0, 1]$ was the resolution coefficient, usually 0.5.

5) Calculate gray weighted relevance r_i

$$r_i = \frac{1}{m} \sum_{j=1}^{m} \xi_{ij}. \qquad (8)$$

6) Evaluation and analysis

According to the size of the grey-weighted correlation degree, the comparison indexes were sorted. A greater correlation degree represented a greater influence of the comparison index on the reference series.

3.4.2 Effect of gradation

Based on the preliminary gradation (Gradation 4) and the molding method determined above, five gradations were

selected from fine to coarse within the range of the upper and lower gradation limits. The air void, compressive strength, Marshall stability, stripping degree and splitting strength were measured to evaluate the effect of different gradations on PUM. The gradation range and test results are shown in Figs. 11 and 12, respectively.

The air voids of gradations 1 and 2 with finer aggregate were significantly lower than those of gradations 3 to 5, indicating the filling effect. The compressive strengths and Marshall stabilities of the coarser gradations 4 and 5

were significantly higher than those of the other gradations, indicating that the coarse aggregate acted as the skeleton in the PUM.

In order to determine the optimum gradation, an extreme differentiation method was also applied to non-dimensionally differentiate the five indexes, as presented in Table 5. The highest standardized total value presented the best comprehensive properties. Therefore, gradation 5 with coarse aggregate was recommended for the mix design of PUM.
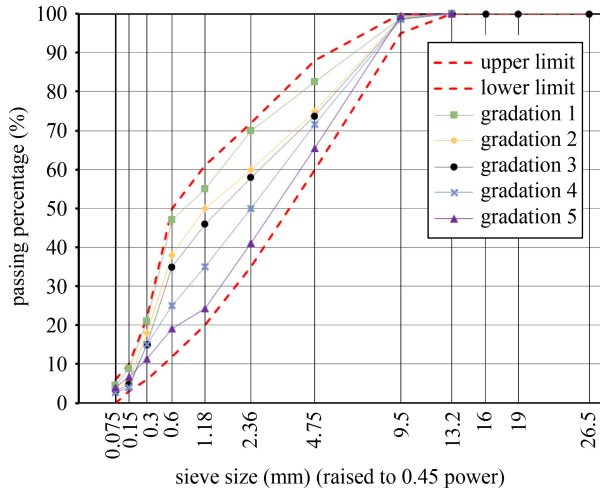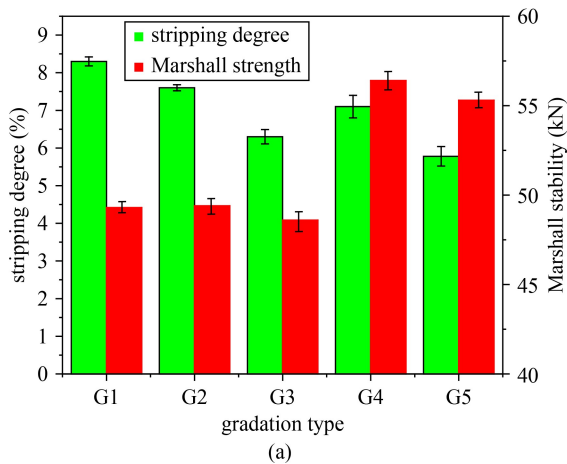
3.4.3   Effect of particle size

In order to analyze the effect of particle size on the properties of PUM, a linear fit was performed on the relationship of each sieve passing rate with air void, compressive strength, Marshall stability, stripping degree and split strength. Since the passing rate of 9.5 mm sieve was over 98% of total material and the passing rate of 0.075 mm sieve was only about 4%, these two sizes was neglected. However, the accuracy of fitted curves with fit goodness ranged from 0.4 to 0.9 could not be evaluated. Therefore, the GRA method was applied to calculate the gray correlation degree value and the weighted average gray correlation degree. The fitting and GRA results are shown in Figs. 13−17.

As shown in Fig. 13, the correlation degree of each sieve to the air void was higher than 0.6, indicating a
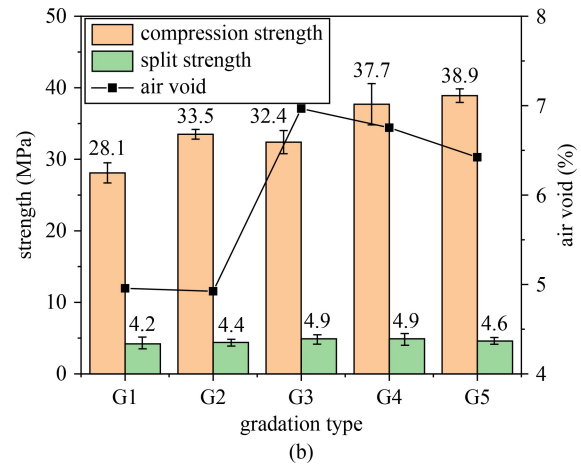

Fig. 11   Gradation range of PUM.

Fig. 12   Performance of PUM with different gradation. (a) Stripping degree and Marshall strength; (b) compression strength, split strength and air void.

Table 5   Min–max range dimensionless results of evaluation indicators

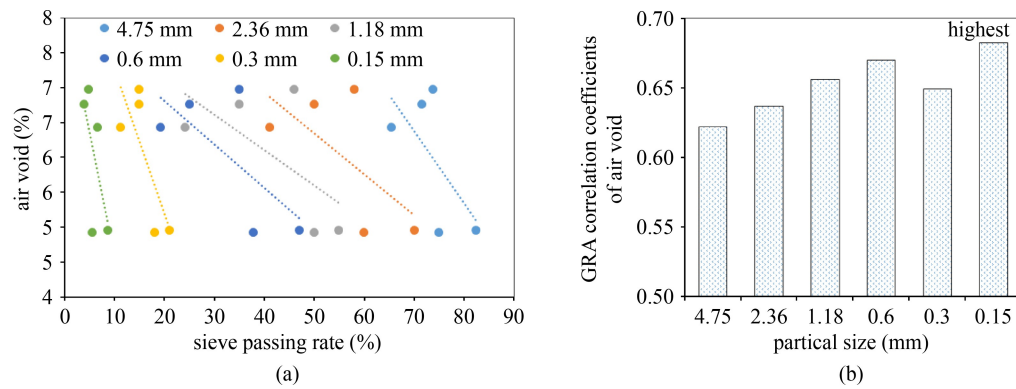| index	air void	compressive strength	Marshall stability	stripping degree	splitting strength	standardized sum
G1	1	0	0.1	0	0	1.1
G2	1	0.5	0.1	0.3	0.3	2.2
G3	0	0.4	0	0.8	1	2.2
G4	0.1	0.9	1	0.5	0.9	3.4
G5	0.3	1	0.9	1	0.6	3.7

Fig. 13   Effect of sieve passing rate on air void. (a) Fitting result; (b) GRA result.
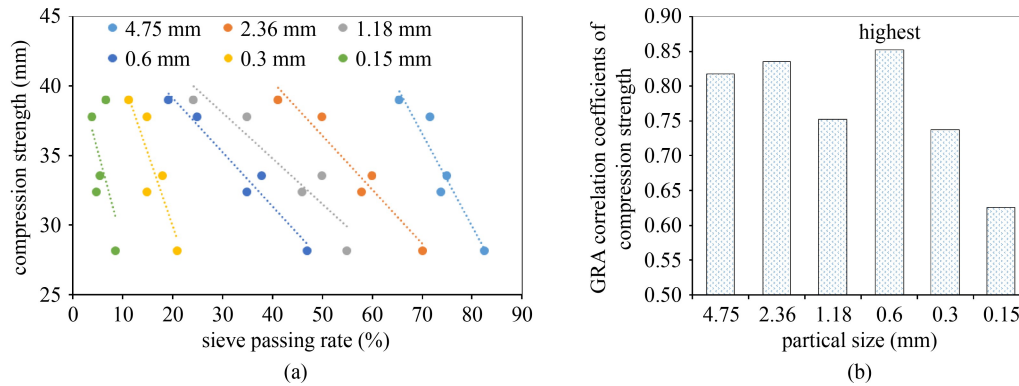

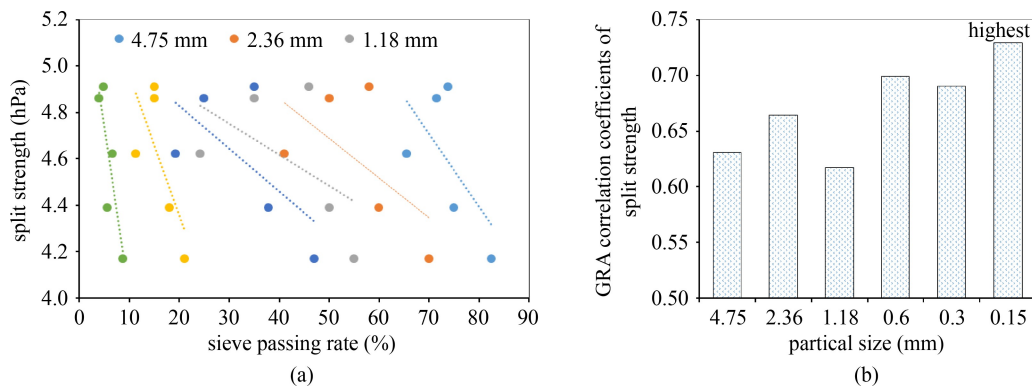**Fig. 14**   Effect of sieve passing rate on compression strength. (a) Fitting result; (b) GRA result.

Fig. 15   Effect of sieve passing rate on split strength. (a) Fitting result; (b) GRA result.
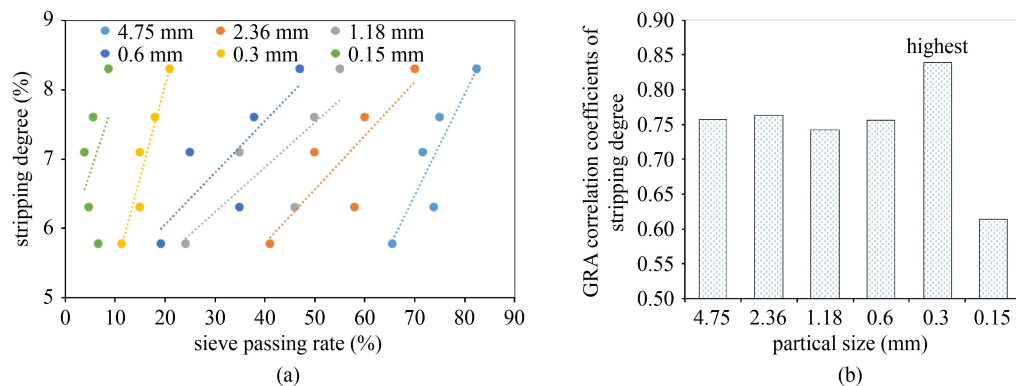

Fig. 16   Effect of sieve passing rate on stripping degree. (a) Fitting result; (b) GRA result.
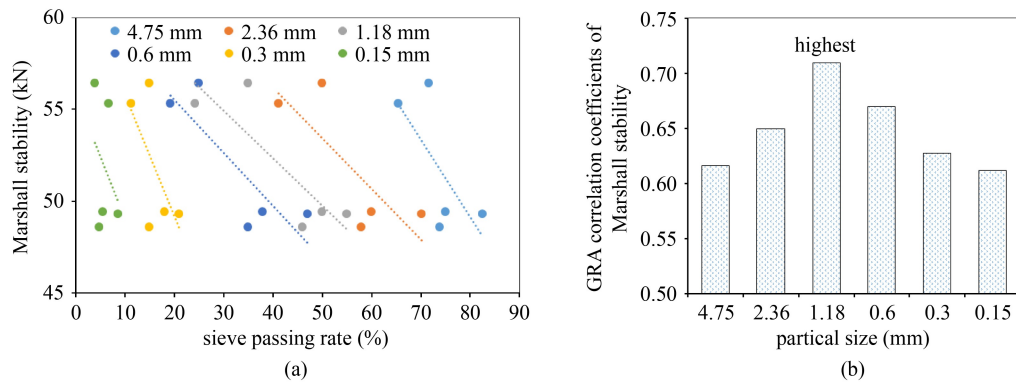
Fig. 17   Effect of sieve passing rate on Marshall stability. (a) Fitting result; (b) GRA result.

great impact of sieve on air void. Comparing each sieve, it was observed that the passing rate of the 0.15 mm sieve presented the greatest influence on the air void, indicating that increasing the passing rate of 0.15 mm sieve could significantly reduce the air void of PUM.

As presented in Fig. 14, the passing rate of the 0.6 mm sieve had the greatest impact on the compressive strength and so reducing the passing rate of 0.6 mm sieve could effectively increase the compressive strength of PUM. The explanation was that the compressive strength mainly came from the embedding skeleton effect of coarse aggregate. The function of fine aggregate was to form mortar with polyurethane binder, filling the skeleton voids, therefore the proportion of fine aggregate needed to be limited.

Figure 15 shows that the passing rate of the 0.15 mm sieve had the greatest influence on the splitting strength with correlation close to 0.75. Reducing the passing rate of the 0.15 mm sieve could significantly improve the splitting strength of PUM, indicating that gradation still contained too many fine aggregates.

As shown in Fig. 16, the correlation value between the 0.3 mm sieve and stripping degree was significantly higher than the other sieves from 0.15 to 4.75 mm, which was close to 0.85. It could be inferred that reducing the passing rate of 0.3 mm sieve was helpful to enhance stripping resistance of PUM. The fine aggregates between 0.15 and 0.3 mm were easy to strip because of insufficient adhesion.

As shown in Fig. 17, the correlation value between passing rate and Marshall stability reached an extreme value at 1.18 mm. The Marshall stability reflected the overall strength in term of the skeleton effect of coarse aggregate and the bonding strength of fine aggregates. Therefore, reducing the 1.18 mm sieve passing rate within the recommended gradation range effectively improved the Marshall stability of PUM.

In summary, increasing the passing rate of the 0.15 mm sieve significantly reduced the air void and splitting strength of PUM. Reducing the passing rate of the 0.3 mm sieve significantly reduced the stripping degree, and controlling the passing rate of the 0.6 and 1.18 mm

sieves effectively improved the compressive strength and Marshall stability.

3.5   Internal structural analyses of polyurethane-bonded mixture

The pore characteristics of pavement materials were the focus of mix design. Figure 18(a) presents the typical reconstruction model of specimens with trimmed surface layer. It shows that the polyurethane binder wrapped the bonded aggregate to form a stable skeleton structure. It could be inferred that the thickness of the polyurethane film affected the mixture performance significantly.

After the reconstruction procedure, the extraction process of air voids was performed. According to the volume sizes, the air voids were extracted and marked with different colors, which are presented in Figs. 18(b)−18(e). Based on the components' voxels numbers, the voids parameters of specimens were further quantitatively analyzed, including air void value, void number and average void diameter. According to the statistical results as shown in Figs. 18(f) and 18(g), the air void of PUM reached 5.39% and the void number of specimens reached 38196. Therefore, the calculated value of average void diameter in PUM was equal to 0.783 mm. In summary, the internal structural details of PUM presented distribution of tiny pores with few connective voids. It could be inferred that PUM had proper waterproof property and high strength.

4   Conclusions

This research investigated and optimized the mix design of PUM for airport thin-overlay technology. The following conclusions can be drawn.

1) PUM with basalt presented favourable mechanical properties: deformation resistance, bonding ability and moisture stability than limestone, and is recommended as the aggregate selection.

2) 60 s dry-mixed time for aggregate and 60 s wet-mixed time for mixture were combined as the
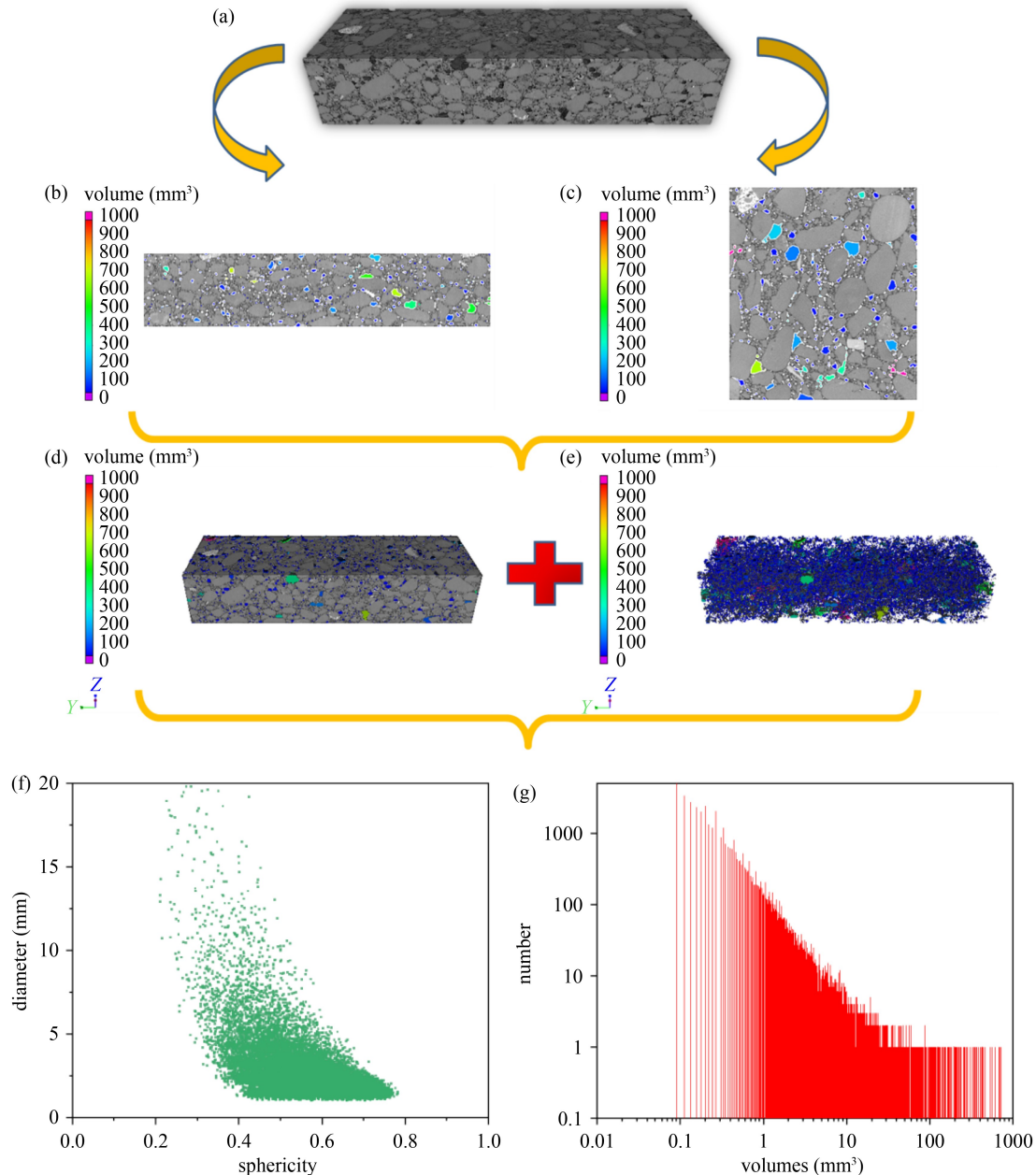
Fig. 18 CT scan analysis with image processing (unit: mm). (a) Specimen reconstructions with surface removal; (b) typical image slices with air analysis, (c) and (d) internal air voids extraction results; (f) sphericity characteristics of air voids; (g) distribution statistics of air voids.

recommended mixing time parameters. The vibratory compaction method with 1 min vibration duration is also suggested for molding PUM.

3) The thermosetting characteristics of polyurethane affected mixture performances significantly. Curing temperature was the main factor affecting performance of PUM, and molding method was the secondary factor. It only took 12 h to reach 75% of the maximum strength at the curing temperature of 50 °C, indicating an efficient curing process and light traffic delay.

4) Increasing the passing rate of a 0.15 mm sieve significantly reduced the air void and splitting strength of PUM. Reducing the passing rate of a 0.3 mm sieve could significantly reduce the stripping degree, and controlling the passing rate of 0.6 and 1.18 mm sieves effectively improves the compressive strength and Marshall stability.

5) Polyurethane binder wrapped the bonded aggregate to form a stable floating dense skeleton structure. The internal structural details of PUM presented a distribution of tiny pores with few connective voids, guaranteeing waterproof property and high strength.

References

1. Liu Y, You Z, Li L, Wang W. Review on advances in modeling and simulation of stone-based paving materials. Construction & Building Materials, 2013, 43(5): 408−417

2. Yuan J, Wang J, Xiao F, Amirkhanian S, Wang J, Xu Z. Impacts of multiple-polymer components on high temperature performance characteristics of airfield modified binders. Construction & Building Materials, 2017, 134(1): 694−702

3. Wang H, Xie P, Ji R, Gagnon J. Prediction of airfield pavement responses from surface deflections: Comparison between the traditional backcalculation approach and the ANN model. Road Materials and Pavement Design, 2021, 22(9): 1930−1945

4. Mirza J, Bhutta M A R, Tahir M M. In situ performance of field-moulded joint sealants in dams. Construction & Building Materials, 2013, 41(8): 889−896

5. Zhao Z, Guan X, Xiao F, Xie Z, Xia P, Zhou Q. Applications of asphalt concrete overlay on Portland cement concrete pavement. Construction & Building Materials, 2020, 264(1): 120045

6. Das P K, Baaj H, Tighe S, Kringos N. Atomic force microscopy to investigate asphalt binders: A state-of-the-art review. Road Materials and Pavement Design, 2016, 17(3): 693−718

7. Li J, Yao S, Xiao F, Amirkhanian S N. Surface modification of ground tire rubber particles by cold plasma to improve compatibility in rubberised asphalt. International Journal of Pavement Engineering, 2022, 23(3): 651−662

8. Li J, Xiao F, Zhang L, Amirkhanian S N. Life cycle assessment and life cycle cost analysis of recycled solid waste materials in highway pavement: A review. Journal of Cleaner Production, 2019, 233(7): 1182−1206

9. Afzal A, Kausar A, Siddiq M. Role of polymeric composite in civil engineering applications: A review. Polymer-Plastics Technology and Materials, 2020, 59(10): 1023−1040

10. Xu L, Li X, Zong Q, Xiao F. Chemical, morphological and rheological investigations of SBR/SBS modified asphalt emulsions with waterborne acrylate and polyurethane. Construction & Building Materials, 2021, 272(9): 121972

11. He Q, Zhang H, Li J, Duan H. Performance evaluation of polyurethane/epoxy resin modified asphalt as adhesive layer material for steel-UHPC composite bridge deck pavements. Construction & Building Materials, 2021, 291(6): 123364

12. Cong L, Yang F, Guo G, Ren M, Shi J, Tan L. The use of polyurethane for asphalt pavement engineering applications: A state-of-the-art review. Construction & Building Materials, 2019, 225(1): 1012−1025

13. Hu Z X, Hu X M, Cheng W M, Zhao Y Y, Wu M Y. Performance optimization of one-component polyurethane healing agent for self-healing concrete. Construction & Building Materials, 2018, 179(9): 151−159

14. Khatoon H, Ahmad S. A review on conducting polymer reinforced polyurethane composites. Journal of Industrial and Engineering Chemistry, 2017, 53(September): 1−22

15. Xu L, Hou X, Li X, Xiao F. Impact of constituent migration on colloid structure and rheological characteristics of emulsified asphalt with self-crosslinking modifiers. Colloids and Surfaces. A, Physicochemical and Engineering Aspects, 2021, 619: 126530

16. Somarathna H M C C, Raman S N, Mohotti D, Mutalib A A, Badri K H. The use of polyurethane for structural and infrastructural engineering applications: A state-of-the-art review. Construction & Building Materials, 2018, 190(4): 995−1014

17. Izquierdo M A, Navarro F J, Martínez-Boza F J, Gallegos C. Bituminous polyurethane foams for building applications: Influence of bitumen hardness. Construction & Building Materials, 2012, 30(1): 706−713

18. Sun M, Zheng M, Qu G, Yuan K, Bi Y, Wang J. Performance of polyurethane modified asphalt and its mixtures. Construction & Building Materials, 2018, 191(2): 386−397

19. Li X, Li J, Wang J, Yuan J, Jiang F, Yu X, Xiao F. Recent applications and developments of Polyurethane materials in pavement engineering. Construction & Building Materials, 2021, 304(10): 124639

20. Min S, Bi Y, Zheng M, Chen S, Li J. Evaluation of a cold-mixed high-performance polyurethane mixture. Advances in Materials Science and Engineering, 2019, 2019(1): 1−12

21. Lu G, Liu P, Törzs T, Wang D, Oeser M, Grabe J. Numerical analysis for the influence of saturation on the base course of permeable pavement with a novel polyurethane binder. Construction & Building Materials, 2020, 240(3): 117930

22. Lu G, Renken L, Li T, Wang D, Li H, Oeser M. Experimental study on the polyurethane-bound pervious mixtures in the application of permeable pavements. Construction & Building Materials, 2019, 202(11): 838−850

23. Chen J, Ma X, Wang H, Xie P, Huang W. Experimental study on anti-icing and deicing performance of polyurethane concrete as road surface layer. Construction & Building Materials, 2018, 161(1): 598−605

24. Gao J, Wang H, Chen J, Meng X, You Z. Laboratory evaluation on comprehensive performance of polyurethane rubber particle mixture. Construction & Building Materials, 2019, 224(3): 29−39

25. Chen J, Yin X, Wang H, Ding Y. Evaluation of durability and functional performance of porous polyurethane mixture in porous pavement. Journal of Cleaner Production, 2018, 188(3): 12−19

26. Cong L, Wang T, Tan L, Yuan J, Shi J. Laboratory evaluation on performance of porous polyurethane mixtures and OGFC. Construction & Building Materials, 2018, 169(1): 436−442

27. Wang D, Schacht A, Leng Z, Leng C, Kollmann J, Oeser M. Effects of material composition on mechanical and acoustic performance of poroelastic road surface (PERS). Construction & Building Materials, 2017, 135(1): 352−360

28. Törzs T, Lu G, Monteiro A O, Wang D, Grabe J, Oeser M. Hydraulic properties of polyurethane-bound permeable pavement materials considering unsaturated flow. Construction & Building Materials, 2019, 212: 422−430